UNIVERSITÀ DEGLI STUDI DI PADOVA

Dipartimento di Fisica e Astronomia "Galileo Galilei"

Corso di Laurea in Fisica

Tesi di Laurea

Establishing perovskite solar cells' efficiencies from first-principles simulations

Relatore

Prof. Paolo Umari

Laureando

Giulio Vittorio Carassai

Anno Accademico 2021/2022

Contents

Introduction

Despite their relatively recent introduction, organic-inorganic lead halide perovskite solar cells have achieved efficiencies typical of cells based on mono-crystalline silicon. Perovskite solar cells still present several unresolved issues, such as their rapid degradation and the presence of toxic lead, which still prevent their viability on the market. Fortunately, perovskite crystalline structure allows for great compositional variety, for example a great effort is being made to replace lead with tin. Perovskite are therefore a very promising candidate for future developments in solar cells technologies.

As a consequence of perovskite great compositional variety, the fundamental physical parameters of these materials take on different values. Most of these parameters can be predicted through first-principle calculations based on density functional theory. It is therefore, at least in principle, possible to theoretically determine the maximum efficiency achievable by a certain device. Consequently, the development of new solar cells can be guided by theoretical predictions.

In this thesis we will determine the power conversion efficiency of simple models of perovskite solar cells with parameters calculated by first principles methods by our group of found present in literature. Specifically, we will consider a *pin* thin film solar cell made of Titanium dioxide, as electron transport material, Methylammonium Lead Iodide (MAPbI3) perovskite, as optical absorber, and Spiro-meOTAD, as hole transport material. We will simulate the cells with SCAPS, a one dimensional solar cell simulation program, and only consider radiative recombination. Finally, we will explore how the cell's fundamental parameters affect efficiency. The perovskite fundamental parameters considered are band gap, affinity, carriers mobility, density of states, and dielectric constant.

This thesis is composed of three chapters. In the first chapter we introduce the models and basic equations of solar cells simulations. In the second chapter we describe perovskites cells and explain the first principle methods used to determine its properties. In the third chapter we review our solar cell simulation and explore how parameters affect the cell's efficiency.

Anche se introdotte da meno di dieci anni, le celle solari basate su perovskiti miste organiche inorganiche hanno raggiunto efficienze tipiche delle celle basati su silicio mono-cristallino. Le celle a perovskite presentano ancora diversi problemi irrisolti, come il loro rapido degrado e la presenza di piombo tossico, che tutt'ora impediscono l'accesso al mercato. Fortunatamente, la stessa struttura cristallina permette una grande varietà composizionale. Ne consegue che parametri fisici fondamentali (come le band gap o le mobilità elettroniche) di tali materiali assumono valori diversi. La gran parte di tali parametri può essere predetta tramite calcoli a principi-primi basati sulla teoria del funzionale della densità (DFT). Questo rende in principio possibile la determinazione teorica della massima efficienza raggiungibile da un certo dispositivo. Di conseguenza lo sviluppo di nuove celle solare può essere guidato da predizioni teoriche. In questa tesi determineremo l'efficienza di semplici modelli di celle solari a perovskite a partire da parametri per le loro componenti fondamentali calcolati a principi-primi dal nostro gruppo o presenti in letteratura. Simuleremo le celle con SCAPS, un programma di simulazione delle celle solari unidimensionale, e a tal fine considereremo solo la ricombinazione radiativa. Infine, esploreremo come i parametri fondamentali della cella influiscono sull'efficienza.

Chapter 1

Modelling Solar Cells

In this chapter we define several fundamental quantities when working with solar cells and the models that explain and predict their behavior.

1.1 Quantities of Interest

The sun emission is strongest in the visible part of the spectrum and resembles that of a 5760K black body. When passing through the atmosphere, sun's radiation is scattered and absorbed at different rates depending on the energy of photon. The result is a general attenuation and slight change in shape of the spectrum. Furthermore, the sun's spectrum, as is perceived on Earth, depends on latitude as well. The standard spectrum for temperate regions is the Air Mass 1.5 spectrum, which models the sun being at an angle of elevation of 42°. Under these conditions, actual irradiance would be attenuated to around 900 W m^{-2}. For the sake of simplicity, however, Air Mass 1.5 spectrum is normalised to have an incident power $P_s = 1000$ W m^{-2}. We will always consider Air Mass 1.5 spectrum as the sun's spectrum in this thesis. We will also refer to incident spectral photon flux density as $b_s(E)$, which is the number of incident photons with energy in the range E to E+dE per unit of area and time.

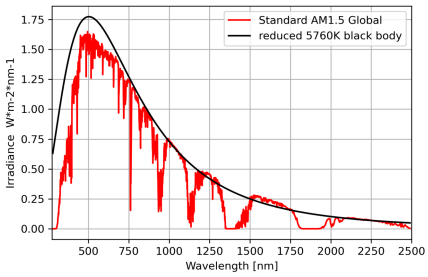

Figure 1.1: Air Mass 1.5 spectrum compared with 5760K black body radiation, reduced by a factor of $4.6 \cdot 10^4$ as suggested in [1].

Modelling an illuminated solar cell as a two ports "black box" circuit allows us to define several important quantities. The short circuit current density (J_{sc}) is the current density drawn when terminals are connected together, while the open circuit voltage (V_{oc}) is the voltage at infinite load resistance. Any load resistance will cause the current density and voltage to be respectively lower than J_{sc} and V_{oc}. The cell's power density is defined as

$$P = JV \tag{1.1}$$

and reaches a maximum for a certain current density $J_m < J_{sc}$ and voltage $V_m < V_{oc}$ when an optimal load is in the circuit. The fill factor (FF) quantifies the "squareness" of the J-V curve and is defines as follows.

$$FF = \frac{J_m V_m}{J_{sc} J_{oc}} \tag{1.2}$$

The cell's power conversion efficiency is therefore defined as

$$\eta = \frac{J_{sc} V_{oc} FF}{P_s} \tag{1.3}$$

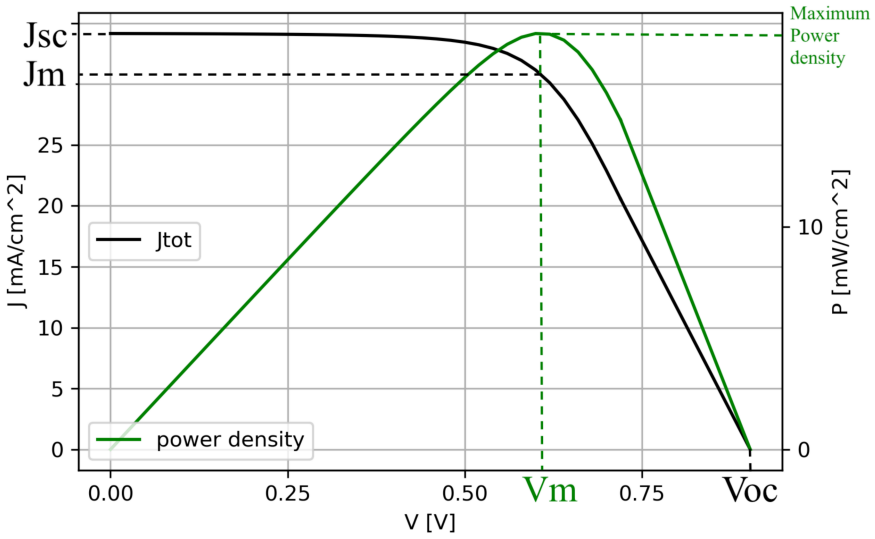

Figure 1.2: Example of simulated solar cell J-V curve and power density. This figure clearly shows that the open circuit voltage and the short circuit current are respectively the maximum voltage and current, while J_m and V_m generate the maximum power density.

Another quantifier of efficiency is quantum efficiency (QE(E)). QE is defined as the probability that an incident photon will generate an electron-hole pair in the cell. Quantum efficiency, therefore, directly relates photocurrent to the sun's photon flux density:

$$J_{sc} = q \int_0^\infty b_s(E) QE(E) dE \tag{1.4}$$

where q is the carrier charge.

1.2 Band Structure

Methylammonium lead iodide perovskites are considered direct band gap semiconductors. As such, we will only discuss direct semiconductors.

The typical energy spectrum of a solid crystal occurs in bands. The highest occupied band at absolute zero is called valence band (VB). The conduction band (CB) is defined as the lowest vacant, or partially vacant, energy band at absolute zero. We refer to VB's maximum as E_V and the CB's minimum as E_C. Semiconductors display a band gap (E_g) between VB and CB in the range of the electron volt. The energy up to which states are completely filled at zero kelvin is called Fermi energy (E_F) and in semiconductors it will lie inside the energy gap. At temperatures above 0K some electrons will have enough kinetic energy to be excited above E_F. In order to define the energy levels' alignment, it is customary to describe energy values in reference to the potential in vacuum (E_{vac}). The vacuum level is defined as the energy to which an electron must be raised in order to be free from all forces from the solid.[1] Therefore, E_V and E_C will lie below vacuum level. Electron affinity (χ), ionization energy (IE) and band gap (E_g) all describe the level alignment in a semiconductor and are defined as follows:

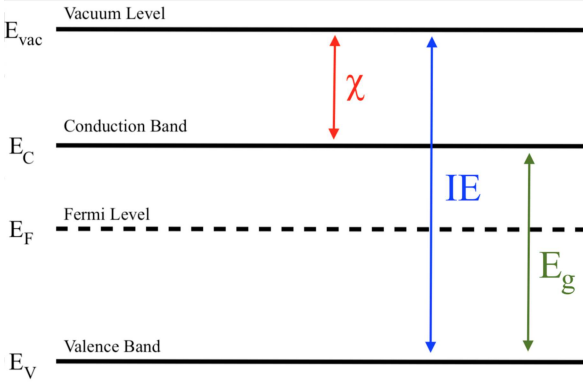

Figure 1.3: Illustration of Fermi and vacuum levels on energy band diagram.

$$\chi = E_{vac} - E_C \tag{1.5}$$

$$E_g = E_C - E_V \tag{1.6}$$

$$IE = E_{vac} - E_V \tag{1.7}$$

As a consequence of Bloch's theorem, the wavevector (k) is a "good quantum number" to describe energy states. In the parabolic band approximation, E(k) is expanded in powers of ($k - k_{0_{C,V}}$) around CB's minimum and VB's maximum up to the Taylor's second order. Notice that since we are considering only direct semiconductors, by definition, CB minimum and VB maximum must occur at the same wave vector $k_{0_{C,V}}$ which we will refer to as k_0.

$$E(k) = E_{0c,v} \pm \frac{\hbar^2 |k - k_0|^2}{2m^*_{c,v}} \tag{1.8}$$

This approximation is particularly insightful because it implicitly defines the carriers effective masses ($m^*_{c,v}$) as

$$\frac{1}{m^*_{c,v}} = \pm \frac{1}{\hbar} \frac{\partial^2 E_{c,v}(k)}{\partial k^2} \tag{1.9}$$

Carrier density of states (DOS) have to obey Pauli's exclusion principle, since electrons are fermions. For a semiconductor in equilibrium, negatively charged carriers (n_c) and positively charged carriers (n_v) state density are

$$n_c = \int\limits_{k \in CB} g_c(k) f(k,r) d^3k \tag{1.10}$$

$$n_v = \int\limits_{k \in VB} g_v(k)(1 - f(k,r)) d^3k \tag{1.11}$$

where $g_i(k)$ is the density of electron states per unit crystal volume (i = v,c), and $f(k,r)$ is the probability that at a given spacial point r the electron state determined by wavevector k is occupied. Conversely, it's natural that $1 - f(k,r)$ has to be the probability that the hole state with wavevector k is occupied. Semiconductors in equilibrium at temperature T follow the Fermi Dirac statistics, so

$$f = f_0(E, E_F, T) = \frac{1}{e^{(E - E_F)/k_B T} + 1} \tag{1.12}$$

where k_B is Boltzmann's constant.
Otherwise, f takes on more complex shapes. If the disturbance is not too great, it is still possible to approximate for quasi thermal equilibrium. Under these assumptions, electrons and holes distribute themselves as if they shared a different Fermi level, called quasi Fermi levels (E_{F_n} and E_{F_p}), and temperature:

$$f_c(k,r) \approx f_0(E, E_{F_n}, T_n) \qquad \text{and} \qquad f_v(k,r) \approx f_0(E, E_{F_p}, T_p) \tag{1.13}$$

Boltzmann's Approximation

For a semiconductor at absolute zero, the valence band is completely filled and the conduction band completely empty. This means that the Fermi level must lie somewhere in the band gap. If E_F is far enough from both band edges, f_0 can be well approximated by the Maxwell-Boltzmann form. In the conduction band when E >> $E_F + k_b T$,

$$f_0 \approx e^{-(E - E_F)/k_B T} \tag{1.14}$$

whereas in the valence band when E << $E_F + k_b T$,

$$1 - f_0 \approx e^{-(E_F - E)/k_B T} \tag{1.15}$$

These approximations allow us to write an analytical solutions to the integrals that define the state densities. Using the parabolic band approximation we find that

$$n_c = N_c e^{(E_F - E_c)/k_B T} \tag{1.16}$$

$$n_v = N_v e^{(E_v - E_F)/k_B T} \tag{1.17}$$

where N_c and N_v are respectively called the effective conduction and valence band density of states and are equal to

$$N_{c,v} = 2(\frac{m^*_{c,v} k_B T}{2\pi\hbar^2})^{3/2} \tag{1.18}$$

where the factor 2 is due to spin degeneracy.
This approximation also allows us to define, using mass action law, the intrinsic carrier density (n_i)

$$n_i^2 = n_c n_v = N_c N_v e^{-E_g/k_B T} \tag{1.19}$$

1.2.1 Generation and Recombination

Generation is an electronic excitation event resulting in the production of charge carriers. Recombination is the opposite process. For every generation event there is an equivalent recombination process due to microscopic reversibility. For solar cells optical generation, i.e. the absorption of photons, is the principal generation process. Recombination, on the other hand, is more diversified. An electron can decay from CB to VB destroying an electron-hole pair, from CB to trap state removing only an electron, or from trap state to VB removing a hole. Furthermore, the way energy is released determines the kind of recombination. In radiative recombination energy is released as a photon, in non-radiative recombination as phonons, i.e. quasi-particles with momentum, while in Auger recombination energy is released as kinetic energy to other free carriers. As mentioned in the abstract, we will only consider radiative recombination.

In a non-degenerate semiconductor, to a good extent, the recombination rate per unit volume can be expressed in terms of carrier densities:

$$U_{rad} = B_{rad}(n_c n_v - n_i^2) \tag{1.20}$$

where B_{rad} is the radiative recombination coefficient and is a property of the material.

$$B_{rad} = \frac{1}{n_i^2}\frac{2\pi}{h^3 c^2}\int_0^\infty \tilde{n}^2 \alpha(E) e^{-E/k_B T} E^2 dE \tag{1.21}$$

where $\tilde{n}$ is the refractive index.

Photogeneration rate is described macroscopically by the absorption coefficient ($\alpha(E)$). In general, for a non uniform material, the intensity as a function of depth (x) will be

$$I(x) = I(0) e^{-\int_0^x \alpha(E,x')dx'} \tag{1.22}$$

It should be noted that for uniform materials this reduces to the simple Beer-Lambert law. Assuming that all absorbed photons generate carriers, then spectral photogeneration rate at depth x, per unit volume, is

$$g(E,x) = b(E,x)\alpha(E,x) = b_s(E)(1 - R(E)) e^{-\int_0^x \alpha(E,x')dx'} \alpha(E) \tag{1.23}$$

Where R is the reflectivity. Therefore, the total generation rate is simply the integral of the spectral generation rates:

$$G(x) = \int g(E,x) dE \tag{1.24}$$

1.2.2 Defects and Doping

Intrinsic semiconductors, perfect crystals without impurities, can be altered by introducing impurities or defects, which change energy levels in the semiconductor. Density and nature of carriers can thus be finely tuned introducing controlled amounts of impurities, i.e. doping the crystal. Doping comes in two variants: n-type and p-type. A semiconductor doped to increase the density of negative carriers compared to positive carriers, is called n-type. Impurities are called donor atoms, since they donate extra electrons to the lattice. The density of carriers is controlled by the density of donor dopants (N_d), and in case of heavy n-doping $n_c \approx N_d$ which in turn means that at equilibrium $n_v \approx n_i^2/N_d$. Conversely, when a semiconductor is doped to increase the density of positive carriers compared, it is called p-type. Impurities are called acceptor atoms, since they reduce valence eletrons. The density of carriers is controlled by the density of acceptor dopants (N_a), and in case of heavy p-doping $n_v \approx N_a$ which in turn means that at equilibrium $n_c \approx n_i^2/N_a$.

Heavy doping can add a tail to CB or VB bands, effectively reducing the band gap. While an undesired consequence of heavy doping is the increase in density of defects, which can act as recombination sites. We will call $\rho_{defect}(n_c, n_v)$ the density of defects.

1.3 Solar Cells' Fundamental Equations

The basic equations that model solar cells are a consequence of two basic principle: the electrostatic potential generated by charge carriers has to obey Poisson's equation and the number of carriers, of each type, must be conserved.

Poisson's equation relates total charge density to the electrostatic potential (ϕ).

$$\nabla^2\phi = -\frac{q}{\epsilon_s\epsilon_0}[-n_c + n_v - N_a + N_d + \rho_{defect}(n_c, n_v)] \tag{1.25}$$

where q is the elementary charge, ϵ_s is the relative dielectric permittivity of the semiconductor, ϵ_0 vacuum permittivity constant, n_c and n_v are respectively the electron and hole density of states, N_a and N_d are respectively the acceptor and donor dopants density and $\rho_{defects}$ is the defects density.

While continuity equations, sometimes referred to as 'book keeping' equations, grant carriers conservation.

$$\frac{\partial n_c}{\partial t} = \frac{1}{q}\nabla \cdot J_n + G_n - U_n(n,p) \tag{1.26}$$

$$\frac{\partial n_v}{\partial t} = -\frac{1}{q}\nabla \cdot J_p + G_p - U_p(n,p) \tag{1.27}$$

Where J_n and J_p are respectively the electron and hole current density, $G_{n,p}$ are the carriers' generation rates and $U_{n,p}$ are the carriers' recombination rates.

Alternatively, Boltzmann transport equations can be used to solve the non equilibrium distribution function. The result are constitutive equations that related current density to mobility, DOS and quasi Fermi levels in semiconductors under bias.

$$J_n = \mu_n n_c \nabla E_{F_n} \tag{1.28}$$

$$J_p = \mu_p n_v \nabla E_{F_p} \tag{1.29}$$

In both cases, the result is a system of coupled differential equations in ϕ, n_c, n_v or ϕ, E_{F_n}, E_{F_p}. Boundary conditions at interfaces and contacts are provided by the external electrical conditions, by the surface recombination condition and by the optical conditions.

The problem has to be solved numerically because the recombination terms, contained in the continuity equations, make the problem non linear in n_c and n_v. Unlike the simpler solutions formulated by Shockley and Queisser,[2] modelling solar cells in general doesn't have analytical solutions. In one dimension, the total cell length is divided in N intervals, and the values of the electric potential ϕ_i and of the electron and hole concentrations $n_{c,i}$ and $n_{v,i}$ at each of the intervals constitute the unknowns of the problem. The problem ultimately boils down to numerically solving 3N nonlinear equations.[3]

Chapter 2

Perovskite Cells

The cell considered in this thesis is a *pin* cell made of perovskite $CH_3NH_3PbI_3$ as the absorber, titanium dioxide (TiO_2) as the electron transport material (ETM) and Spiro-Ome TAD as the hole transport material (HTM). In this chapter we first discuss the characterizing principles of *pin* cell. We then define the fundamental properties of the aforementioned used materials and the first principles methods used to determine such properties. Temperature is always kept as a constant at 300K.

2.1 Structure of *pin* Cells

pin junctions are a typical design of perovskite-based thin film solar cells. *pin* cells can remedy perovskite's low carrier mobility. They are composed of three layers: the hole transport material (HTM), the absorber and the electron transport material (ETM). The hole transport material is a p-type semiconductor and therefore has the highest EC and EV among the three layers. The absorber is an intrinsic semiconductor and it's the main contributor to photogeneration. Finally, the electron transport material is instead an n-type semiconductor and therefore has the lowest EC and EV among the three layers.

This stairs-like design of the energy levels drives carriers, generated in the absorber, towards contacts through their respective transport material. Electrons are driven towards the ETM and holes towards the HTM by quasi-Fermi levels' gradients as asserted by the constitutive equations (equations 1.27 and 1.27). The overall effect is a decrease in recombination rates, compared to a design that only includes the absorber.

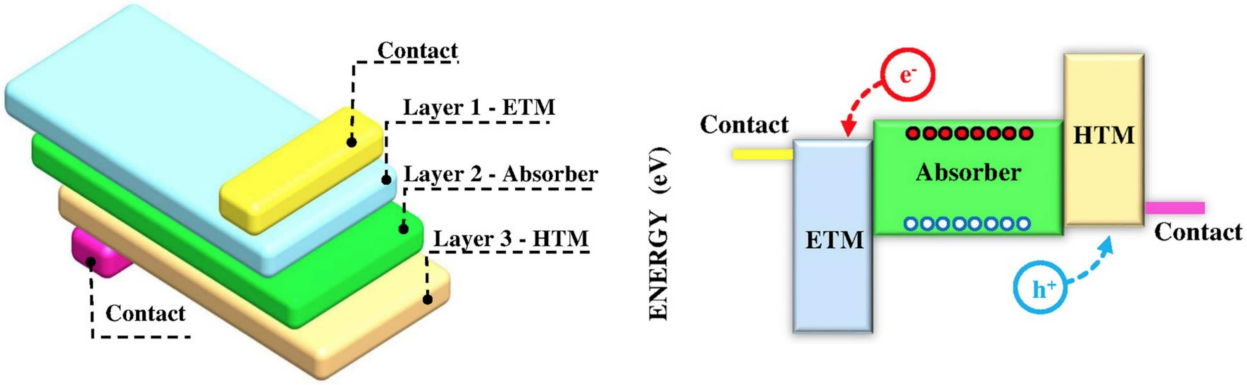

Figure 2.1: Schematic illustration of *pin* cells' structure and energy alignment.[4]

It follows that this design is preferred in materials where minority carrier diffusion lengths are short, which is the case of perovskites due to their low carrier mobility. Maximizing efficiency involves balancing generation and recombination rates, both of which are a function of the absorber's thickness.

For these reasons, optimizing cell geometry, i.e. the layers lengths, is a crucial step when defining a cell's efficiency.

It's also worth noticing ETM and HTM usually aren't as effective in photogeneration as the absorber. For this reason it's also crucial that they do not contribute significantly in light absorption.

2.2 Properties of the Materials

The choice of using titanium dioxide and Spiro-Ome TAD as the cell's transport materials was motivated by two reasons. First, their properties are well suited and compatible with MAPbI3. Secondly, they have become the gold standard of perovskite based solar cell simulations. Therefore, Titanium dioxide and Spiro-Ome TAD also allowed us to be consistent with the literature.

2.2.1 Transport Materials Properties

All TiO_2 and Spiro-Ome TAD properties, except for Titanium dioxide's affinity, were selected from literature.[5] TiO_2 was considered in it's Anatase phase. Titanium dioxide's affinity was determined by *GW* calculations by Carla Verdi, Edoardo Mosconi, Filippo De Angelis, Margherita Marsili, and P. Umari.[6] The GW method is an approximation where the expansion of the self-energy, in terms of the single particle Green's function and the screened Coulomb interaction, is truncated after the first term. This first principles simulation was implemented using the Quantum Espresso package.

Material Properties	TiO_2	Spiro-Ome TAD
Bandgap (E_g) [eV]	3.26	3.06
Electron affinity (χ) [eV]	4.5	2.05
Relative dielectric permittivity (ϵ_s)	10	3
Effective CB DOS (N_c) [$1/cm^3$]	2e17	2.8e19
Effective CB DOS (N_v) [$1/cm^3$]	6e17	1e19
Electron mobility (μ_n) [cm^2/Vs]	100	1e-4
Hole mobility (μ_p) [cm^2/Vs]	25	2e-4
Donor density (N_d) [$1/cm^3$]	1e17	0
Acceptor density (N_a) [$1/cm^3$]	0	1e18
Electron thermal velocity ($v_{e^-}^{th}$) [cm/s]	1e7	1e7
Hole thermal velocity ($v_{h^+}^{th}$) [cm/s]	1e7	1e7
Radiative recombination coefficient (B_{rad}) [cm^3/s]	2.3e-9	2.3e-9

Table 2.1: Transport materials properties.

2.2.2 Perovskite Properties

Perovskite's properties were all determined by first principles calculations. We considered MAPbI3 in its tetragonal form, common at room temperature, and with methylammonium iodide (MAI) coverage (θ) which we'll first consider as constant ($\theta = 0.5$), and then as variable to investigate how it affects the cell's efficiency. MAI-rich surfaces induce an up-shift of the perovskite's energy bands, which are use to improve hole transfer at the perovskite/HTL interface.

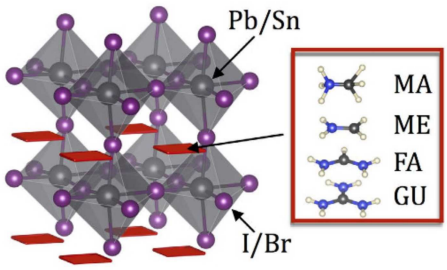

Figure 2.2: Composition of the considered perovskite.[7]

Meggiolaro *et al.* investigated the effects of MAI coverage on MAPbI3's ionization energies using Density Functional Theory (DFT). DTF is a first principle method based on low velocities approximation of the Dirac equation. The assumptions of DFT are not entirely justified since MAPbI3 contains lead which has rather high velocities. Spin orbit coupling (SOC) can however improve results. Meggiolaro *et al.*

used HSE06 functional approximation and considered SOC. Interestingly, Meggiolaro *et al.* estimate of surface formation energy (SFE) also showed that MAI-terminated perovskite displays a higher stability,[8] which is one of the crucial challenges for market viability of perovskite based solar cells.

Material Properties	MAPbI3
Bandgap (E_g) [eV]	1.67
Electron affinity (χ) [eV]	3.83
Relative dielectric permittivity (ϵ_s)	7.1
Effective CB DOS (N_c) [$1/cm^3$]	2.078e+18
Effective VB DOS (N_v) [$1/cm^3$]	3.136e+18
Electron mobility (μ_n) [cm^2/Vs]	50
Hole mobility (μ_p) [cm^2/Vs]	75
Electron relative effective mass (m_e^*)	0.19
Hole relative effective mass (m_h^*)	0.25
Electron thermal velocity ($v_{e^-}^{th}$) [cm/s]	1.75e7
Hole thermal velocity ($v_{h^+}^{th}$) [cm/s]	1.57e7
Radiative recombination coefficient (B_{rad}) [cm^3/s]	6.072e-06

Table 2.2: Absorber's properties.

Perovskite's band gap, dielectric function, mobility, effective masses where determined by Umari *et al.* with relativistic GW methods that incorporate spin-orbit coupling (SOC).[9] Previously used Density Functional Theory (DFT) tended to underestimate band gaps, while SOC-GW's estimates are within ± 0.1 eV compared to experimental values. This method also allowed to calculated optical properties, in particular real and imaginary dielectric function (ϵ_1 and ϵ_2) with high precision. Indeed, the program actually provided the dielectric tensor, so the values considered were the three Cartesian directions averages.

We considered Meggiolaro *et al.* estimate of perovskite's electron affinity, since we were interested in MAI terminated MAPbI3. Meggiolaro and Umari's used similar methods and produced consistent results (E_g varies by 0.1 eV between the two studies), therefore we deduced that both studies can be simultaneously considered.

The other properties were determined as follows.
Thermal velocities only depends on the carriers' effective masses.

$$v_{e^-/h^+}^{th} = \sqrt{\frac{8k_BT}{2\pi m_{e^-/h^+}^*}} \tag{2.1}$$

Absorption coefficient, as a function of energy, was calculated from the dielectric function. Indeed, refractive index ($\tilde{n}$) and extinction coefficient $\tilde{k}$ are directly linked to the dielectric function since it can be inferred from the definition of the complex index of refraction that

$$\begin{cases} \epsilon_1 = \tilde{n}^2 - \tilde{k}^2 \\ \epsilon_2 = 2\tilde{n}\tilde{k} \end{cases} \tag{2.2}$$

Once we determined the extinction coefficient, the absorption coefficient follows from the following relation.

$$\alpha(E) = \frac{2E\tilde{k}}{\hbar c} \tag{2.3}$$

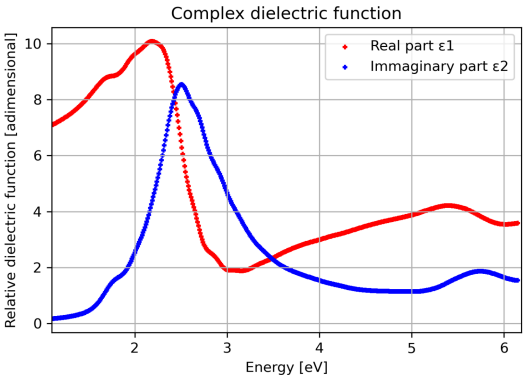

Figure 2.3: Simulated complex dielectric function.

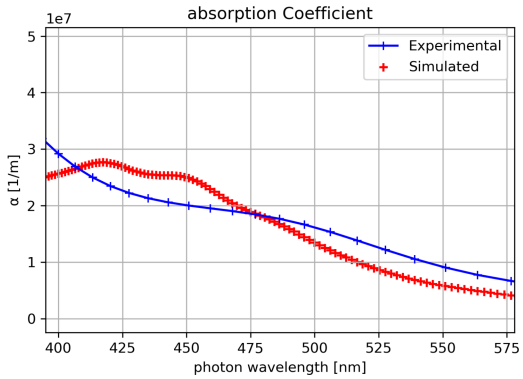

Figure 2.4: Comparison between simulated and experimental Perovskite absorption coefficient.[10]

Effective density of states were calculated assuming parabolic band approximation and using Eq. 1.18, since they are only a function of the effective masses and temperature. This also allowed us to calculate the intrinsic carrier density, which in turn was used to determine the radiative recombination coefficient B_{rad} using Eq. 1.21.

Chapter 3

SCAPS Simulation of Perovskites Cells

In this chapter we will first describe how simulations of the considered perovskite cell were implemented, including cell geometry optimization. Secondly, we will explore the effects of several of the absorber's properties on power efficiency.

3.1 Solar Cell Definition and Simulation

We defined the solar cell on SCAPS using the aforementioned data. It was decided to illuminate the cell from the HTM's side because it generated superior cell performance. Materials grading was set to uniform and no defects were introduced in the cell. Furthermore, having chosen uniform grading, tunnelling was not considered since it seemed unnecessary.

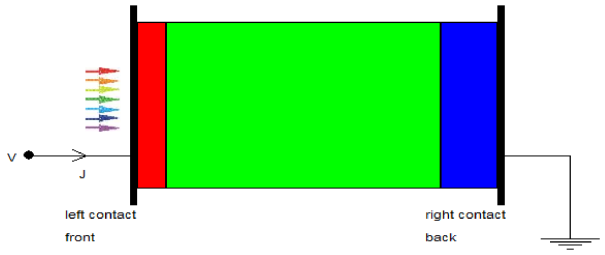

Figure 3.1: Example of *pin* cell diagram on SCAPS.

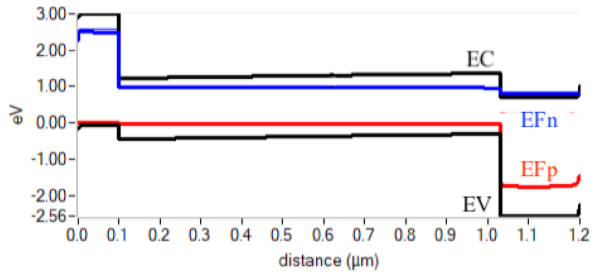

Figure 3.2: Example of *pin* cell energy bands.

Figure 3.2. clearly shows *pin* cells' typical stair-like band alignment between layers.

3.1.1 Contacts and Band Alignment at Interfaces

Contacts' work functions were chosen to satisfy the following relations, which are necessary to ensure the proper operation of the cell.[4]

$$\begin{cases} \chi_{ETM} \leq \Phi_{BC} \\ \chi_{HTM} \leq \chi_P \\ \Phi_{FC} \leq \chi_{HTM} + E_{g,HTM} \\ \chi_{HTM} + E_{g,HTM} \leq \chi_P + E_{g,P} \end{cases} \tag{3.1}$$

Where Φ_{FC} is the front contact work function and Φ_{BC} is the back contact work function. The resulting optimized values were $\Phi_{FC} = 4.95$ eV and $\Phi_{BC} = 4.7$ eV. All the relations that did not involve contacts were already verified. This is convincing evidence that cell definition was reasonable.

3.1.2 Cell's Geometry Optimization

The HTM layer, absorber, and ETM layer thicknesses were optimized employing a "greedy" approach. The three thicknesses were considered independent variables when determining the efficiency. We therefore assumed the the order in which the thicknesses were optimized was inconsequential. This was the most computationally cost effective way of proceeding. The computational cost of three dependent variables scales as N^3, since every combination needs to be simulated. Comparing cubic scaling to our method's linear scaling, therefore, made our method more appealing.

We proceeded optimizing first the HTM thickness having set the initial values of thicknesses of the absorber and ETM layer equal to 1 μm and 150 nm respectively. These values were consistent with optimal thicknesses found in the literature.[5] The iteration process launched to optimize HTM thickness consisted in a broad scan varying the layer thickness from 1nm to 1300nm, followed by a fine tuning around the maximum. Then using the obtained optimum value of HTM, similar iterations were carried out to compute the absorber optimal thickness and the the ETM optimal thickness. Interestingly, as it can be seen in the figures, efficiency was very correlated with the first optimized thicknesses, while remained rather constant when optimizing ETM layer thickness. ETM's optimal thickness was chosen as the peak of the "inverted parabola" visible in figure 3.4. This, however, was a rather arbitrary choice since η only varied by 0.0001% as the ETM thickness varied between 160 nm and 220 nm.
The optimal parameters were HTM thickness 80 nm, absorber thickness 1.93 μm and ETM thickness 195 nm, which determined a cell efficiency of 18.71%.

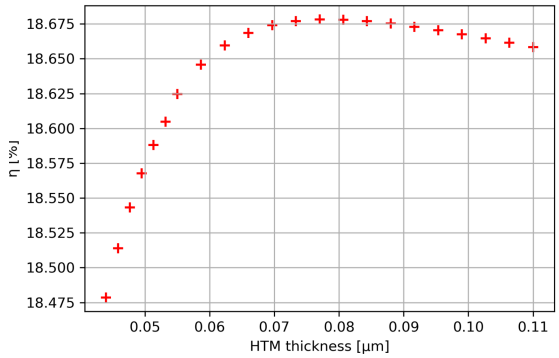

Figure 3.3: HTM thickness effects on efficiency.

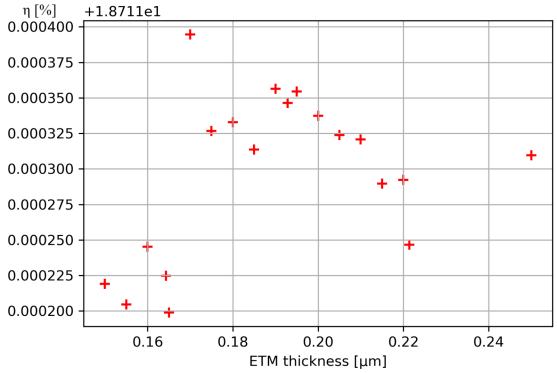

Figure 3.4: ETM thickness effects on efficiency.

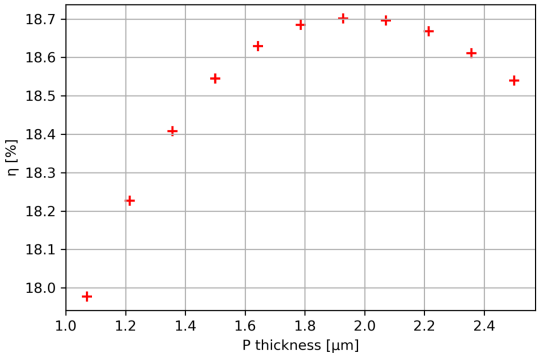

Figure 3.5: Perovskite thickness effects on efficiency.

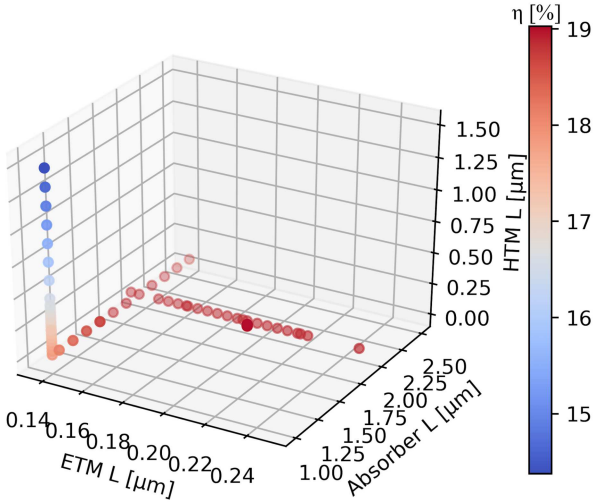

Figure 3.6: Cell's geometry optimization.

3.1.3 Recombination coefficient's effects on optimal absorber's thickness and cell efficiency

It is also worth noticing that theoretical predictions suggest that the optimal absorber thickness is highly correlated with the recombination coefficient B_{rad}. As the absorber thickness increases we expect carrier generation to increase. However, as suggested by Eq. 1.23, the total carrier generation rate however decreases exponentially in function of depth, while recombination rate is constant. Therefore, we expect efficiency to increase as thickness increases as long as generation rate is greater than recombination rate. After that point, efficiency saturates and decreases as recombination rate becomes dominant.

In order to confirm that the decrease of η beyond 1.93 μm is related to current loss due to the carrier recombination, we ran simulations using two other different values of the recombination constant: $B_1 = 9.072 \cdot 10^{-6} cm^3/s$ and $B_2 = 3.072 \cdot 10^{-6} cm^3/s$.

As expected changes in recombination coefficient have two effects. Higher B_{rad} values cause the optimal thickness to be shorter since more recombination would happen in the same length. At the same time, overall maximum efficiency is also be affected and decreases as B_{rad} increases. This is indeed what happens as attested by figure 3.7.

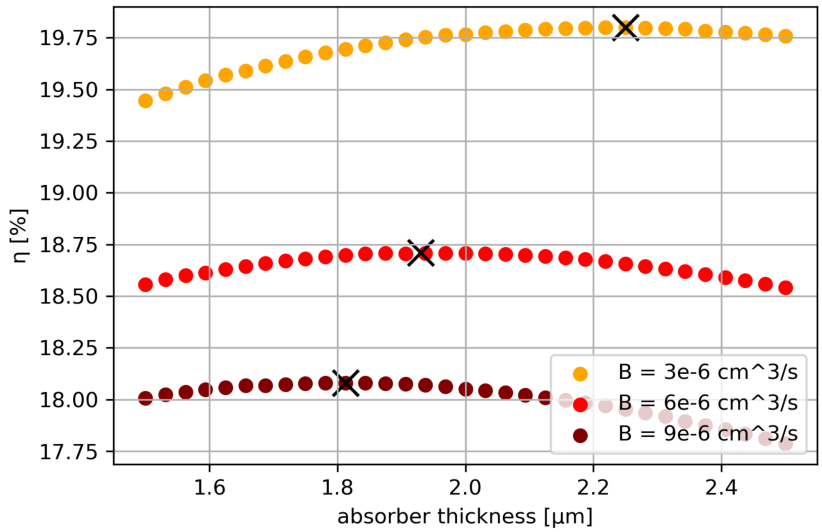

Figure 3.7: Recombination coefficient effects on efficiency and optimal absorber thickness. The maximums efficiencies are marked by X signs.

3.1.4 Results

The optimized cell had V_{oc} and J_{sc} similar to those found in literature, while efficiency and fill factor were sensibly lower. Other papers indeed report 80% fill factors and 25% efficiency.[7] This discrepancy may be caused by the our absorption coefficient simulation, which was indeed lower than the experimental in the range between 480 nm and 575 nm, which are exactly the wavelengths where the solar spectrum is highest.

The cell's JV curve shows that generation current remains constant, while it's the radiative recombination current - the only recombination current since we only considered radiative recombination - that determines the cell's current.

V_{oc} [V]	0.903
J_{sc} [mA/cm^2]	34.2
FF [%]	60.7
η [%]	18.71

Figure 3.8: IV characteristics of the simulated cell.

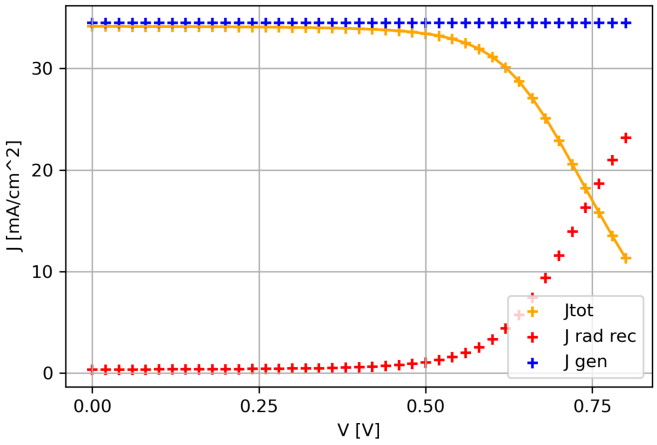

Figure 3.9: JV curves of the simulated cell.

Quantum efficiency is well adapted for the sun spectrum. As expected, it sharply decreases for wavelengths higher than 742nm, i.e. for energies lower than 1.67 eV which is the energy gap.

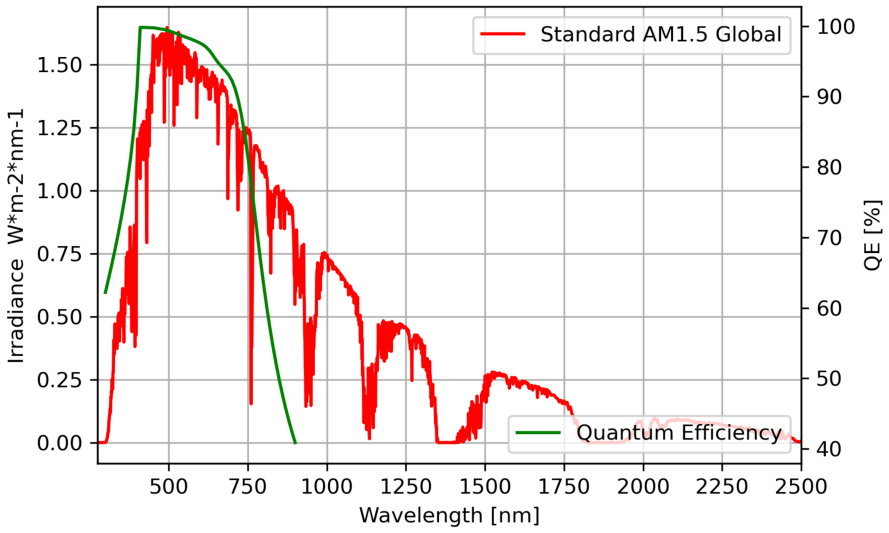

Figure 3.10: Cell efficiency dependency from perovskite energy gap and affinity.

3.2 Efficiency Dependence on Cell's Parameters

In this section we explored how several of the absorber's parameters affect overall cell efficiency. The inquired properties were energy levels (E_g and χ), electron and hole mobility, effective density of states and relative dielectric permittivity.

3.2.1 Perovskite Energy Bands and MAI coverage

We investigated efficiency's dependency on perovskite's band alignment. To do so we simulated 2500 cells with E_g ranging from 1.5 eV to 2 eV and χ from 3.67 eV to 4.2 eV. In the explored region of the $E_g - \chi$ plane efficiency decreases rapidly when E_g and χ decrease, it decreases less rapidly at high affinities and stays rather constant around 18% for a large sector. The cell we previously defined lies of course in the high efficiency sector.

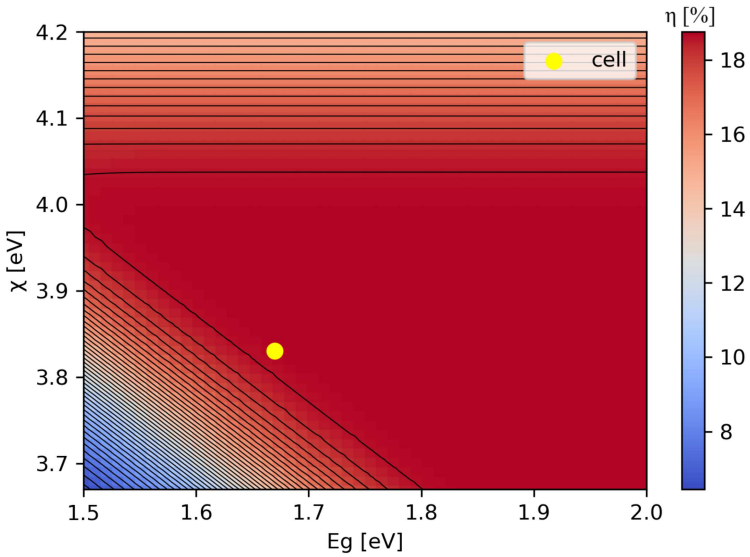

Figure 3.11: Efficiency dependency from energy gap and affinity. Black lines are level sets with the same efficiency.

In order to explain the low efficiencies at low E_g and χ, we should first remember that $E_{vac} - E_V = \chi + E_g$. Therefore, simulation on the same $y = -x + c$ diagonal all share the same E_V. If the absorber's E_V is too low however, the *pin* design becomes counter productive because holes tend to be trapped in the absorber until they recombine, consequently reducing the efficiency.

Horizontal equiefficent lines on top of the graph show the other area where efficiency decreases. In this case we have to remember that $E_{vac} - E_C = \chi$. Therefore simulation on the same horizontal line share the same E_C. Similarly as before, if χ becomes too large, E_C decreases. If this happens electrons will tend to be trapped in the absorber until they recombine, consequently reducing the efficiency.

MAI Coverage Effects on Efficiency

We simulated MAI coverage effects on cell efficiency assuming that MAI coverage only affects band gap and affinity. To this end, we employed Meggiolaro's simulations. We only simulated data with $\theta \geq 0.25$ because of SCAPS limits in simulating cells.

Efficiency appeared to be very strongly correlated to MAI coverage, with the best performance for $\theta = 0.5$. Interestingly, high MAI coverage seems to be detrimental to the cell's efficiency since for $\theta > 0.625$ we see a collapse in efficiency to very low levels.

Meggiolaro's paper also included a simulation of water effects on band alignment (at $\theta = 0$). Our efficiency simulations seemed to imply that water actually improves the cells performance, although

these results are actually inconclusive since we only varied E_g and χ while water affects a large plethora of other properties.

MAI coverage (θ)	E_g [eV]	χ [eV]	η [%]
0.250	1.62	4.15	16.36
0.375	1.69	3.84	18.75
0.500	1.67	3.83	18.71
0.625	1.74	3.33	4.15
0.750	1.77	3.09	0.94
0.875	1.78	2.98	0.07
1.00	1.87	3.07	2.59

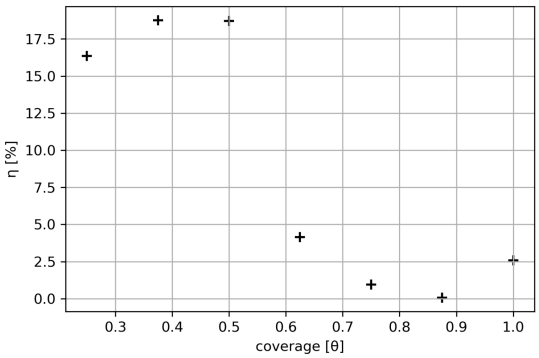

Figure 3.12: Efficiency dependency by MAI coverage.

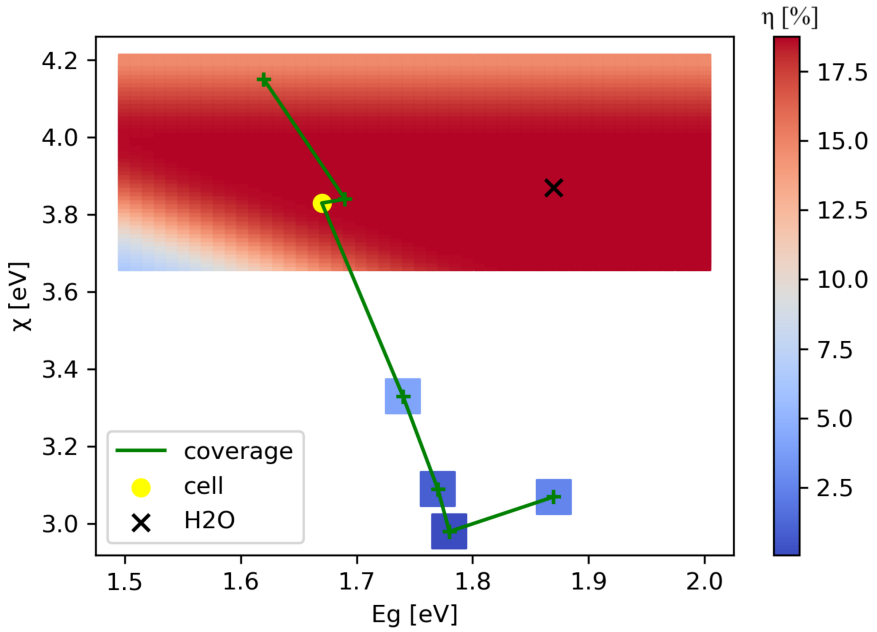

Figure 3.13: MAI coverage effects on efficiency.

3.2.2 Mobility

We simulated the effects of the absorber layer's electron and hole mobility on efficiency. To do so we simulated 2200 cells with μ_e and μ_h varying exponentially between 1 cm^2/Vs and 100 cm^2/Vs.

As expected, as the electron and hole mobility increase, so does efficiency. The constitutive equations indeed

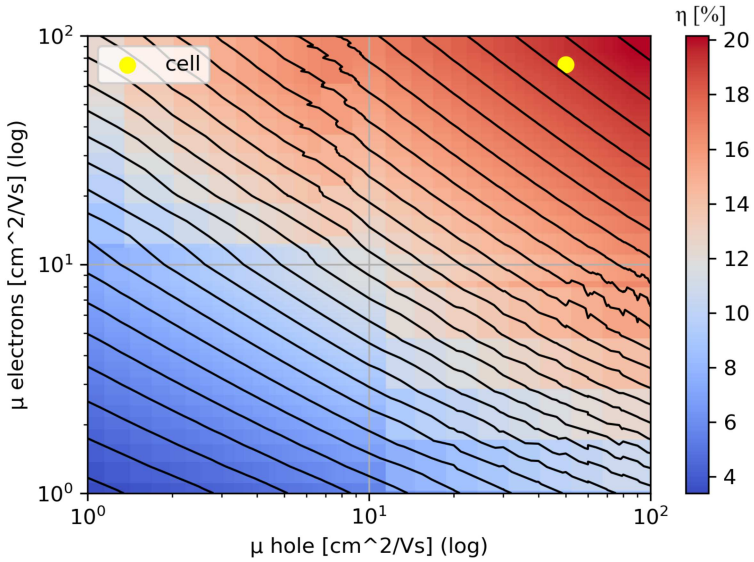

Figure 3.14: Hole and electron perovskite mobility effects on efficiency. Black lines are level sets with the same efficiency.

Interestingly, the constant spacing between equiefficient lines in the bi-log graph, figure 3.14, and the simulations linear behavior in the logarithmic graphs, figures 3.15 and 3.16, are both empirical evidence that simulated efficiency is proportional to the logarithm of mobility.

Upon closer inspection, figures 3.15 and 3.16 actually feature piece-wise functions made of 2 linear pieces. This can be explained considering that there are two mobility involved: electrons' mobility and holes' mobility. So when one becomes dominant there is a change in behavior. Indeed the lines with $\mu = 10\ cm^2/Vs$ are the straightest because the two mus are always comparable.

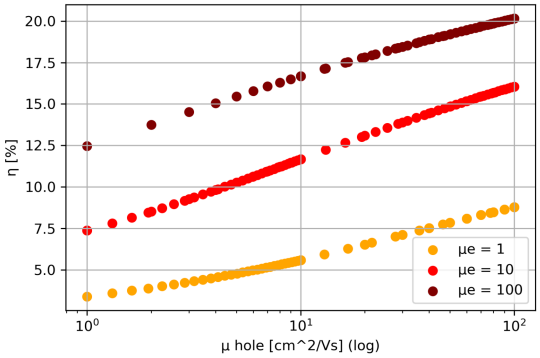

Figure 3.15: Effects of hole mobility on efficiency at different fixed electron mobility.

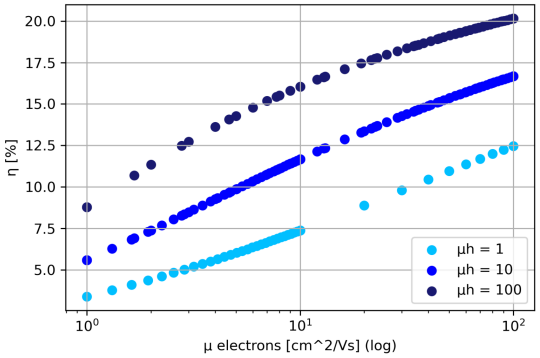

Figure 3.16: Effects of electron mobility on efficiency at different fixed hole mobility.

3.2.3 Effects of Doping

We simulated the effects of doping the absorber layer on the cell's efficiency by varying the effective density of states (N_c and N_v). To do so we simulated 1600 cells with N_c and N_c varying exponentially between $10^{16}\ cm^{-3}$ and $10^{22}\ cm^{-3}$.

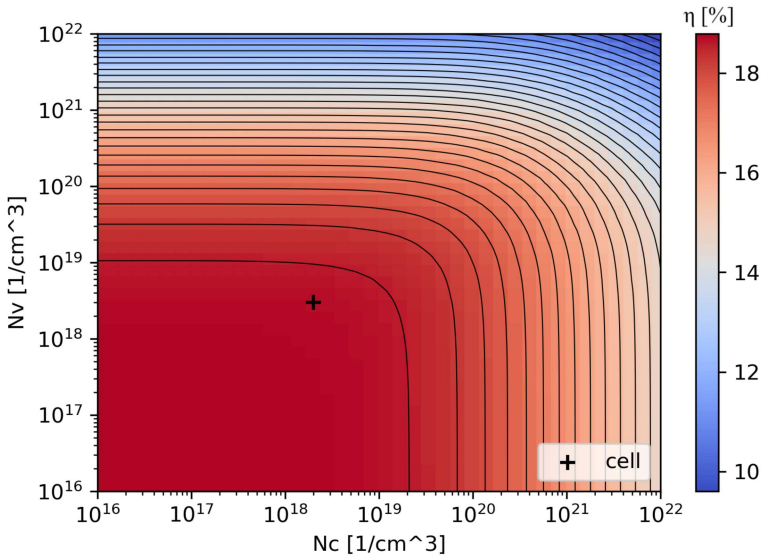

Figure 3.17: Perovskite doping effects on efficiency. Black lines are level sets with the same efficiency.

Efficiency stays rather constant at low densities but decreases sharply as $N_{c,v}$ surpasses 10^{19} cm^{-3}. This behavior can be explained, once again, as a consequence of the *pin* cell design. Heavily doping the absorber causes drift currents from the carrier transport materials to the absorber, thus opposing the photocurrents.

3.2.4 Dielectric Constant

Lastly, we testes a large spectrum of dielectric permittivity values, ranging from 0.4 to 80, to explore the limits of how ϵ_{rel} affects efficiency. Our simulations show that dielectric permittivity effects on efficiency are rather negligible. Efficiency only varies by 0.008%

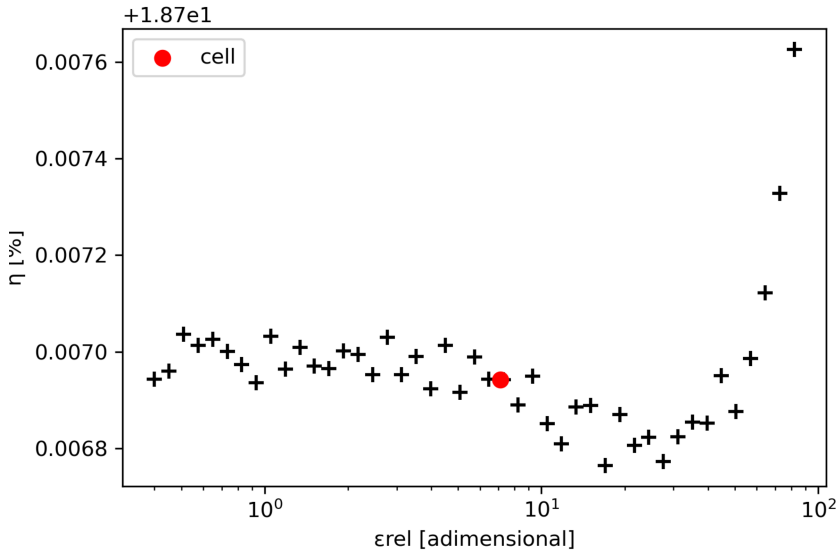

Figure 3.18: Absorber's dielectric permittivity effects on efficiency.

A possible explanation of this incongruity might be the results are actually distorted because a change in epsilon would also cause a change in the absorption index, which was not considered, which would greatly influence generation rates and therefore efficiency.

Conclusion

Our first-principle simulations of solar cells showed promising results, and made parameter dependencies rather intuitive and easy to visualize.

The considered TiO2-MAI terminated MAPbI3-Spiro-Ome TAD cell had a optimal efficiency of 18.71%, which was slightly lower than other groups first principles simulated efficiency.[7] While the open circuit voltage and short circuit current were 0.903 V and 34.2 mA/cm2, which were very similar to other groups first principles simulations results.

The cell's fundamental parameters simulated effects on efficiency were always consistent theoretical predictions.

Bibliography

[1] Jenny Nelson. *The Physics of Solar Cells*. Imperial College Press, 2005.

[2] William Shockley and Hans J. Queisser. "Detailed Balance Limit of Efficiency of p-n Junction Solar Cells". In: *Journal of Applied Physics* 32.3 (Mar. 1961), pp. 510–519.

[3] Marc Burgelman et al. "Modeling Thin-film PV Devices". In: *Applied research* (2004).

[4] Ahmer Baloch et al. "Full space device optimization for solar cells". In: *Scientific Reports* 7 (Sept. 2017), p. 11984. DOI: 10.1038/s41598-017-12158-0.

[5] Mohammad I. Hossain, Fahhad H. Alharbi, and Nouar Tabet. "Copper oxide as inorganic hole transport material for lead halide perovskite based solar cells". In: *Solar Energy* 120 (2015), pp. 370–380.

[6] Carla Verdi et al. "Alignment of energy levels in dye/semiconductor interfaces by *GW* calculations: Effects due to coadsorption of solvent molecules". In: *Phys. Rev. B* 90 (15 Oct. 2014), p. 155410.

[7] Dmitry Vinichenko Efthimios Kaxiras Oscar Grånäs. "Establishing the limits of efficiency of perovskite solar cells from first principles modeling". In: *Scientific Reports* (2016).

[8] Daniele Meggiolaro et al. "Energy Level Tuning at the MAPbI3 Perovskite/Contact Interface Using Chemical Treatment". In: *ACS Energy Letters* 4.9 (2019), pp. 2181–2184.

[9] P. Umari, E. Mosconi, and F. De Angelis. "Relativistic GW calculations on CH3NH3PbI3 and CH3NH3SnI3 Perovskites for Solar Cell Applications". In: *Scientific Reports* (2014).

[10] P. Löper et al. "Complex Refractive Index Spectra of CH3NH3PbI3 Perovskite Thin Films Determined by Spectroscopic Ellipsometry and Spectrophotometry". In: *The Journal of Physical Chemistry Letters* (2015).